SCIENTIFIC REPORTS

OPEN

A numerical treatment of MHD radiative flow of Micropolar nanofluid with homogeneous-heterogeneous reactions past a nonlinear stretched surface

Received: 26 January 2018
Accepted: 4 August 2018
Published online: 20 August 2018

Dianchen Lu[1], M. Ramzan[1,2,4], Shafiq Ahmad[3], Jae Dong Chung[4] & Umer Farooq[1,5]

The impact of nonlinear thermal radiation in the flow of micropolar nanofluid past a nonlinear vertically stretching surface is investigated. The electrically conducting fluid is under the influence of magnetohydrodynamics, heat generation/absorption and mixed convection in the presence of convective boundary condition. The system of differential equations is solved numerically using the bvp4c function of MATLAB. To authenticate our results, two comparisons with already studied problems are also conducted and an excellent concurrence is found; hence reliable results are being presented. Complete deliberation for magnetite nanofluid with Ferric Oxide (Fe_3O_4) nanoparticles in the water-based micropolar nanofluid is also given to depict some stimulating phenomena. The effect of assorted parameters on velocity, homogeneous-heterogeneous reactions, temperature and micropolar velocity profiles are discussed and examined graphically. Moreover, graphical illustrations for the Nusselt number and Skin friction are given for sundry flow parameters. It is examined that temperature distribution and its associated boundary layer thickness increase for mounting values of the magnetic parameter. Additionally, it is detected that the Nusselt number decays when we increase the values of the Biot number.

Flows over stretched surfaces have various engineering and industrial applications like the extrusion of plastic sheets, extraction of polymer, glass blowing, drawing of wires, paper production and rubber sheets[1]. The pioneering work of flow of Newtonian fluid over a moving rigid surface by Sakiadis[2] has motivated the follower scientists and researchers to reveal more thought-provoking ideas in this core area. Sakiadis's idea was improved by Crane[3] who considered a stretching sheet instead of a rigid surface. This was followed by an excellent research article by Gupta and Gupta[4] who studied the effect of heat transfer on a viscid fluid past a stretching sheet. Later, Chakrabarti and Gupta[5] improved the work of Gupta and Gupta[4] by analyzing the flow of viscid fluid past a stretching sheet in the presence of magnetohydrodynamics. Devi and Ganga[6] discussed dissipation impacts on nonlinear flow with magnetohydrodynamics past a permeable medium. Considering the importance of flows over stretched surfaces, scientists and researchers are encouraged even today to look for new ideas. Some salient contributions in this regard include a study by Hsiao[7] who discussed the impacts of Ohmic dissipation and MHD on the flow of viscoelastic fluid through a stretched sheet. Ibrahim *et al.*[8] deliberated the magnetohydrodynamics nanofluid flow over a stretching surface. Lin *et al.*[9] inspected the Pseudoplastic flow of nanofluid past a time-dependent stretching surface under the influence of variable thermal conductivity, viscous dissipation, and Joule heating. The nanofluid flow over the stretching sheet, with the effects of stagnation point, heat source/sink and electro magnetohydrodynamic with slip boundary condition, was analyzed by Hsiao[10]. Hayat *et al.*[11] found

[1]Department of Mathematics, Faculty of Science, Jiangsu University, Zhenjiang, Jiangsu, China. [2]Department of Computer Science, Bahria University, Islamabad Campus, Islamabad, 44000, Pakistan. [3]Department of Mathematics, Quaid-I-Azam University, Islamabad, 44000, Pakistan. [4]Department of Mechanical Engineering, Sejong University, Seoul, 143-747, Korea. [5]Department of Mathematics, COMSATS University, Park road, Tarlai Kalan, Islamabad, 45550, Pakistan. Correspondence and requests for materials should be addressed to M.R. (email: mramzan@bahria.edu.pk)

the series solution for the third-grade fluid flow with an impact of chemical reaction past an unsteady stretching surface. Malvandi *et al.*[12] obtained the numerical solution of the flow of variable nanofluid in the neighborhood of a stagnation point with Navier's slip condition. Numerical solution of flow of MHD nanofluid past a shrinking/stretching surface in a spongy medium near a stagnation point was discussed by Khalili *et al.*[13]. The flow of Jeffrey fluid over a linearly stretching sheet was examined by Hayat *et al.*[14]. Hayat *et al.*[15] also analyzed the Powell Eyring fluid flow past a stretched surface mounted at an angle with effects radiation and non-uniform sink/source. Ahmadi *et al.*[16] inspected a detailed study of nanofluid flow past an unsteady extended surface. Chen *et al.*[17] found the numerical solution of Maxwell fluid flow past a time-dependent stretched surface. Hua and Su[18] studied the time-dependent flow over a stretched surface in a moving fluid with impacts of frictional and Ohmic heating. Hayat *et al.*[19] explained the flow of viscous fluid past an exponential stretched surface with slip condition and magnetohydrodynamics. Waqas *et al.*[20] found numerical solution of the micropolar fluid flow with effects of mixed convection, magnetohydrodynamics and convective boundary conditions past a nonlinear stretched surface. Lu *et al.*[21] debated the flow of magneto-hydrodynamic Carreau nanofluid flow numerically with impacts of nonlinear thermal radiation with zero mass flux condition past a radially stretching sheet.

Flows involving effects of the chemical reactions have gained the attraction of the researchers and scientists. Applications of these flows in various processes may include the production of ceramics and polymers, chemical processing, fibrous insulations, water and air pollutions and molecular diffusion of species. Chemical reactions are labeled as homogeneous- heterogeneous (h & h) reactions. The domain in the case of heterogeneous reactions is restricted however it covers the entire phase uniformly. Combustion and catalysis cover both h & h reactions. Moreover, the heterogeneous catalyst is found in the solid phase while homogeneous catalyst exists in gaseous and liquid phases. Recent investigations involving the impacts of h & h reactions include a study by Imran *et al.*[22] who discussed the flow of Casson fluid numerically with effects of h & h reactions with magnetohydrodynamics and viscous dissipation. Hayat *et al.*[23] examined analytical solution of 2D micropolar fluid with h & h reactions and magnetohydrodynamics. The flow of 3D Oldroyd-B fluid flow with nonlinear thermal radiation and homogeneous-heterogeneous (h-h) reactions is discussed by Lu *et al.*[24]. Abbas and Sheikh[25] numerically found the solution of Ferrofluid with nonlinear slip condition and h & h reactions. Nadeem *et al.*[26] explored the influence of magnetic dipole numerically past a stretched cylinder with h & h reactions. Raju *et al.*[27] found dual solutions of Jeffrey fluid flow numerically with the impact of h & h reactions. Imad *et al.*[28] examined the Prandtl fluid flow with h & h reactions past a linearly stretched surface.

During the last few years, the heat transport phenomenon in fluid flows got broad consideration owing to its varied applications in engineering and technology. Nanofluids are comprised of nanometer-sized particles, named as nanoparticles, and some usual base fluids. The nanoparticles used in nanofluids are characteristically composed of oxides, metals, carbon nanotubes, or carbides. The concept of nanofluids was first time given by Choi[29] Later, Keblinski *et al.*[30] experimentally and numerically proved that the thermal conductivity of nanofluids is prominent in comparison to the ordinary base fluids. Consequently, usage of nanofluids in engineering applications like in domestic refrigerators, nuclear reactors, chiller, heat exchangers, engine cooling and vehicle thermal management has immensely increased. More about applications of nanofluids may be found in[31]. Our intention here is to report different latest studies highlighting varied aspects of nanofluids. These may include an investigation by Nadeem and Noor[32] who investigated the impact of Cattaneo-Christov mass and heat flux in a nanofluid implanted in a spongy medium. Nadeem and Lee[33] used an exponentially stretching surface to deliberate the flow of nanofluid. Sheikholeslami[34] described the ethylene glycol nanofluid flow in the presence of thermal radiation past a porous enclosure. Nadeem *et al.*[35] considered the influence of mass and heat transfer on peristaltic flow of a nanofluid between eccentric cylinders. Sheikholeslami[36] used complex geometry to discuss the impact of the electric field on the hydrothermal conduct of nanofluid. In the presence of porous medium Raju and Sandeep[37] investigated radiative magnetohydrodynamic Jeffrey nanofluid flow past a cone with chemical reaction.

A literature survey indicates that abundant studies are available discussing the flow of micropolar fluid flow with different geometries. Comparatively less work is done with micropolar nanofluid flow and as far as our knowledge is concerned no study so far is conducted for the flow of micropolar nanofluid with h-h reactions over a nonlinear vertically stretched sheet. Additional features of nonlinear thermal radiation and heat absorption/generation coefficient are also added characteristics towards its novelty. Numerical solution of the transformed equations is gained by utilizing the built-in function bvp4c. A complete parametric investigation is conducted using the graphical depiction of different controlling flow parameters on axial velocity, h-h reactions, temperature, microrotation velocity, and concentration profile. Additionally, the local Nusselt and friction factor numbers are graphed and dissected for increasing dynamical parameters. A comparison to a previously done study is also conducted to validate our presented results. An excellent alignment is obtained in this regard which proves that our results are indubitable.

Theory and Flow Field Analysis

We assume an incompressible, steady two-dimensional boundary layer flow of micropolar nanofluid past a nonlinear vertically stretching surface with stretching velocity $u(x) = U_w(x) = cx^n$ along *x-axis*, where c is a constant. The flow is under the impacts of the nonlinear magnetic field, nonlinear thermal radiation, heat absorption/generation coefficient, and h & h reactions. The strength of the magnetic field is taken as $B(x) = B_0 x^{(n-1)/2}$ acting in a normal direction to *y-axis*. We also assume that in qusient micropolar nanofluid both base fluid (water) and nanoparticles (Fe_3O_4) are in thermal equilibrium and there is no chance of slip occurrence. The temperature at the surface is T_w where the ambient temperature is taken as T_∞ as $y \to \infty$. Schematic diagram of the flow problem is depicted in Fig. 1.

The model for homogeneous (isothermal cubic autocatalytic) and heterogeneous reactions with two chemical species A* and B* was proposed by Merkin[38] and Chaudhary and Merkin[39,40] is given by

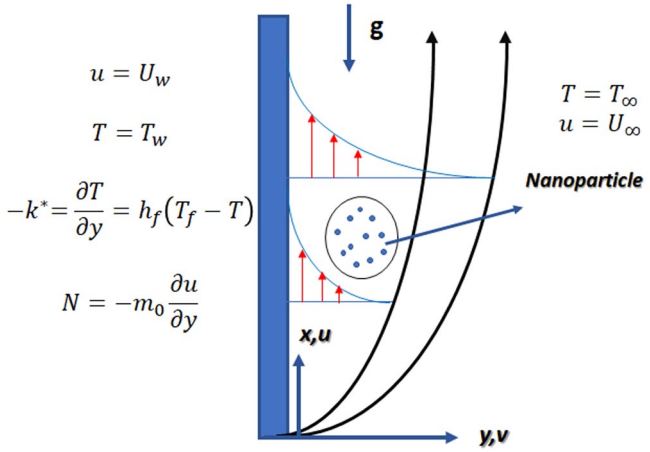

Figure 1. Schematic diagram of the model.

$$A^* + 2B^* \rightarrow 3B^*, \qquad \text{rate} = k_c a b^2, \tag{1}$$

$$A^* \rightarrow B^*, \qquad \text{rate} = k_s a, \tag{2}$$

where the concentration of chemical species B^* and A^* are given by b and a and $k_i, (i = c, s)$ are the rate quantities. Both reaction forms are considered as isothermal. Applying the boundary layer approximation, the continuity, micropolar, energy and concentration equations can be stated as follows:

$$\frac{\partial u}{\partial x} + \frac{\partial v}{\partial y} = 0, \tag{3}$$

$$u\frac{\partial u}{\partial x} + v\frac{\partial u}{\partial y} = \left(\upsilon_{nf} + \frac{\kappa}{\rho_{nf}}\right)\frac{\partial^2 u}{\partial y^2} + \frac{\kappa}{\rho_{nf}}\frac{\partial N}{\partial y} + g_1\beta(T - T_\infty) - \frac{\sigma_{nf}B^2(x)}{\rho_{nf}}u, \tag{4}$$

$$u\frac{\partial N}{\partial x} + v\frac{\partial N}{\partial y} = \frac{y^*}{\rho_{nf}j}\frac{\partial^2 N}{\partial y^2} - \frac{\kappa}{\rho_{nf}j}\left(2N + \frac{\partial u}{\partial y}\right), \tag{5}$$

$$u\frac{\partial T}{\partial x} + v\frac{\partial T}{\partial y} = \alpha_{nf}\frac{\partial^2 T}{\partial y^2} - \frac{1}{(\rho c_p)_{nf}}\frac{\partial q_r}{\partial y} + \frac{Q_0}{(\rho c_p)_{nf}}(T - T_\infty), \tag{6}$$

$$u\frac{\partial a}{\partial x} + v\frac{\partial a}{\partial y} = D_A\frac{\partial^2 a}{\partial y^2} - k_c a b^2, \tag{7}$$

$$u\frac{\partial b}{\partial x} + v\frac{\partial b}{\partial y} = D_B\frac{\partial^2 b}{\partial y^2} + k_c a b^2. \tag{8}$$

These equations are supported by the following boundary conditions

$$\begin{aligned} &u|_{y=0} = U_w(x) = cx^n, \; v|_{y=0} = 0, \quad N = -m_0\left.\frac{\partial u}{\partial y}\right|_{y=0}, \\ &-k_1^*\left.\frac{\partial T}{\partial y}\right|_{y=0} = h_f(T_f - T), \quad D_A\left.\frac{\partial a}{\partial y}\right|_{y=0} = k_s a, \quad D_B\left.\frac{\partial b}{\partial y}\right|_{y=0} = -k_s a, \\ &u|_{y\rightarrow\infty} \rightarrow 0, \quad N|_{y\rightarrow\infty} \rightarrow 0, \quad T|_{y\rightarrow\infty} \rightarrow T_\infty, \quad a|_{y\rightarrow\infty} \rightarrow a_0, \quad b|_{y\rightarrow\infty} \rightarrow 0, \end{aligned} \tag{9}$$

where $y^* = j\left(\mu_{nf} + \frac{\kappa}{2}\right)$ shows the spin gradient viscosity. The symbols g_1, β, κ, $B(x)$, N, j, Q_0, (D_A, D_B), (k_c, k_s), m_0, k^*, h_f, T_f, n are the gravitational acceleration, thermal expansion coefficient, magnetic parameter, coefficient of volumetric thermal expansion, microrotation velocity, micro inertia, the variable volumetric rate of heat source, diffusion coefficients, rate constants, boundary parameter, mean absorption coefficient, convective heat transfer coefficient, convective fluid temperature, and power law index respectively. It is pertinent to mention that the

Physical properties	Base fluid (water)	Fe_3O_4
C_p $(J/kg\,K)$	4179.00	670
ρ (kg/m^3)	997.100	5180
K_1 (W/mK)	0.61300	9.7
σ (Ωm)	1.4700	1163.1

Table 1. Thermo-physical characteristics of the base fluid (water) and nanoparticles (Fe_3O_4).

value of n directly relates to the shape of the surface. For $n=1$, the surface is flat, for $n>1$, the surface is inner concave and for $n<1$, the surface is outer convex. Similarly, the values n can also predict the motion of the fluid. The values $n=1$, $n<1$, and $n>1$, represent the linear motion of the fluid with constant velocity decelerated motion and accelerated motion respectively. In Eq. (6), nonlinear thermal radiation heat flux q_r via Rosseland's approximation is given by

$$q_r = \frac{4\sigma^*}{3k^*}\frac{\partial T^4}{\partial y} = \frac{16\sigma^* T^3}{3k^*}\frac{\partial T}{\partial y} \tag{10}$$

The values of the specific heat C_p, the density ρ, the thermal conductivity K_1 and the electric conductivity σ of the base fluid (water) and the magnetite nanoparticles (Fe_3O_4) (water) are given in Table 1.

The mathematical form for the thermophysical properties are

$$\begin{aligned}
\mu_{nf} &= \frac{\mu_f}{(1-\phi)^{2.5}}, \quad \frac{\rho_{nf}}{\rho_f} = 1-\phi+\phi\frac{\rho_s}{\rho_f},\\
\frac{\sigma_{nf}}{\sigma_f} &= 1-\frac{3\phi\left[1-\frac{\sigma_s}{\sigma_f}\right]}{\left[2+\frac{\sigma_s}{\sigma_f}\right]+\phi\left[1-\frac{\sigma_s}{\sigma_f}\right]},\\
\alpha_{nf} &= \frac{k_{nf}}{(\rho C_p)_{nf}}, \quad \frac{(\rho C_p)_{nf}}{(\rho C_p)_f} = (1-\phi)+\phi\frac{(\rho C_p)_s}{(\rho C_p)_f},\\
\frac{k_{nf}}{k_f} &= \frac{(2k_f+k_s)-2\phi(k_f-k_s)}{(2k_f+k_s)+\phi(k_f-k_s)}.
\end{aligned} \tag{11}$$

Similarity transformation. Using the following transformations

$$\begin{aligned}
&\psi = f(\eta)\sqrt{\frac{2\nu_f x u_e(x)}{n+1}}, \quad \eta = y\sqrt{\frac{(n+1)u_e(x)}{2x\nu_f}}, \quad N = cx^n\sqrt{\frac{(n+1)u_e(x)}{2x\nu_f}}g(\eta),\\
&u = cx^n f'(\eta), \quad v = -\sqrt{\frac{(n+1)\nu_f c x^{n-1}}{2}}\left\{f(\eta)+\left(\frac{n-1}{n+1}\right)\eta f'(\eta)\right\},\\
&T_\infty + (T_w - T)\theta(\eta) = T, \quad a = a_0 h, \quad b = a_0\varphi.
\end{aligned} \tag{12}$$

The requirement of continuity equation is inevitably satisfied, and Eqs (4) to (8) become

$$\begin{aligned}
&\left(\frac{1}{(1-\phi)^{2.5}(1-\phi+\phi\frac{\rho_s}{\rho_f})}+\frac{K}{(1-\phi+\phi\frac{\rho_s}{\rho_f})}\right)f''' + ff'' - \left(\frac{2n}{n+1}\right)f'^2 + \frac{K}{\left(1-\phi+\phi\frac{\rho_s}{\rho_f}\right)}g'\\
&+\frac{2}{n+1}\left(\lambda\theta - \frac{M(\sigma_{nf}/\sigma_f)}{\left(1-\phi+\phi\frac{\rho_s}{\rho_f}\right)}f'\right) = 0,
\end{aligned} \tag{13}$$

$$\begin{aligned}
&\left(\frac{1}{(1-\phi)^{2.5}(1-\phi+\phi\frac{\rho_s}{\rho_f})}+\frac{K}{2(1-\phi+\phi\frac{\rho_s}{\rho_f})}\right)g'' + g'f - \left(\frac{3n-1}{n+1}\right)gf' - \frac{2K}{(n+1)(1-\phi+\phi\frac{\rho_s}{\rho_f})}\\
&(2g+f'') = 0,
\end{aligned} \tag{14}$$

$$\begin{aligned}
&\left(\frac{k_{nf}}{k_f}+R_d(1+(\theta_w-1)\theta)^3\right)\theta'' + \mathrm{Pr}\left(1-\phi+\phi\frac{(\rho C_p)_s}{(\rho C_p)_f}\right)\left(f\theta' - \frac{2\gamma}{n+1}\theta\right)\\
&+3R_d(\theta_w-1)(1+(\theta_w-1)\theta)^2\theta'^2 = 0,
\end{aligned} \tag{15}$$

$$\frac{1}{S_c}h'' + fh' - \frac{2k_1}{n+1}h\varphi^2 = 0, \tag{16}$$

$$\frac{\delta}{S_c}\varphi'' + f\varphi' + \frac{2k_1}{n+1}h\varphi^2 = 0, \tag{17}$$

and the boundary conditions in Eq. (9) yield the following form

$$\begin{aligned} f(\eta) &= 0,\ f'(\eta) = 1,\ \theta'(\eta) = -B_i(1-\theta(\eta)),\ g(\eta) = -m_0 f'(\eta), \\ h'(\eta) &= k_2 h(\eta), \quad \delta\varphi'(\eta) = -k_2 h(\eta) \quad \text{as} \quad \eta = 0, \\ \theta(\eta) &= 0,\ f'(\eta) = 0,\ g(\eta) = 0,\ \varphi(\eta) = 0,\ h(\eta) = 1, \quad \text{at} \quad \eta \to \infty, \end{aligned} \tag{18}$$

where prime designate the derivative with respect to η. The parameters k_2, M, K, R_d, γ, k_1, S_c, δ, B_i, λ represent the strength of heterogeneous reaction, magnetic parameter, micropolar parameter, radiation parameter, heat generation parameter, the strength of homogeneous reaction, Schmidt number, the ratio of diffusion coefficient, Biot number and mixed convection parameter respectively are defined as follows

$$\begin{aligned} &\lambda = \frac{Gr_x}{\mathrm{Re}_x^2}, \quad K = \frac{\kappa}{\mu_f}, \quad M = \frac{\sigma_f B^2(x)}{c\rho_f}, \quad \mathrm{Pr} = \frac{\nu_f}{\alpha_f}, \quad R_d = \frac{16\sigma^* T_\infty^3}{3kk^*}, \\ &\mathrm{Re}_x = \frac{u_w x}{\nu_f}, \quad Gr_x = \frac{g_1\beta(T_w - T_\infty)x^3}{\nu_f^2}, \quad \gamma = \frac{Q_0}{c(\rho C_p)_f}, \quad S_c = \frac{\nu_f}{D_A}, \\ &k_1 = \frac{{a_0}^2 x k_c}{U_w}, \quad k_2 = \frac{k_s}{D_A}\sqrt{\frac{x\nu_f}{U_w}}, \quad B_i = \frac{h_f}{k_1^*}\sqrt{\frac{x\nu_f}{U_w}}, \quad \delta = \frac{D_A}{D_B}. \end{aligned} \tag{19}$$

In general, the chemical species A and B won't be identical, nevertheless, we can expect that these will be equivalent in size[38]. Here, we suppose that the diffusion species coefficients D_B and D_A are identical, *i.e.,* $\delta = 1$, thus we have

$$\varphi(\eta) + h(\eta) = 1. \tag{20}$$

Now applying the above property, Eqs (16) and (17) and their corresponding boundary condition take the form

$$\frac{1}{S_c}h'' + fh' - \frac{2k_1}{n+1}h(1-h)^2 = 0, \tag{21}$$

$$h'(0) = k_2 h(0), \quad h(\infty) \to 1. \tag{22}$$

Friction factor and local Nusselt number. The dimensional forms of the C_f (skin friction coefficient) and Nu_x (the local Nusselt number) are categorized as

$$C_f = \frac{2\tau_w}{\rho_f u_w^2}, \quad Nu_x = \frac{xq_w}{k_1^*(T_f - T_\infty)}. \tag{23}$$

Now the surface heat flux (q_w) and surface shear stress (τ_w) are assumed as:

$$\tau_w = \left(\frac{\partial u}{\partial y}(\kappa + \mu_{nf}) + \kappa N\right)_{y=o}, \quad q_w = -\left(\frac{\partial T}{\partial y}\right)_{y=0} k_{nf} + (q_r)_{y=0}. \tag{24}$$

Using Eqs (12) and (24) in Eq. (23), we acquire

$$\begin{aligned} \mathrm{Re}_x^{1/2} C_f &= \sqrt{\frac{n+1}{2}}\left(\frac{1}{(1-\varphi)^{2.5}} + (1-m_0)K\right)f''(0), \\ \mathrm{Re}_x^{-1/2} Nu_x &= -\frac{k_{nf}}{k_f}\sqrt{\frac{n+1}{2}}\theta'(0), \end{aligned} \tag{25}$$

where $\mathrm{Re}_x = \frac{u_w x}{\nu_f}$ is the local Reynolds number.

Results and Discussion

The numerical solution, of Eqs (13, 14, 15, 21) with associated boundary conditions Eqs (18) and (22), is obtained using MATLAB built-in function bvp4c. For this purpose, initially, we have converted the third and second order differential equations to the first-order ordinary differential equations using new parameters. The built-in function bvp4c requires an initial supposition and the tolerance for the current problem is given as 10^{-7}. Considering

n	M	$-f''(0)$	
		Reddy[41]	Present result
1	0.5	0.865956	0.86595
	01	1.097058	1.09705
	02	1.753714	1.75371
	03	2.744580	2.74458
2	0.5	0.950290	0.95029
	01	1.101523	1.038900
	02	1.572680	1.57268
	03	2.429416	2.42941

Table 2. Comparison of $-f''(0)$ with[41] for numerous values of n and M when $\Pr = 0.7, \phi = 0.0$.

n	$-f''(0)$	
	Cortell[42]	Present result
0.0	0.627547	0.627547
0.2	0.766758	0.766758
0.5	0.889477	0.889477
0.75	0.953786	0.953786
1.0	1.0	1.0
1.5	1.061587	1.061587
3.0	1.148588	1.148588

Table 3. Comparison of $-f''(0)$ with[42] for various values of n in the absence of the micropolar nanofluid and h-h reactions when $M = 0 = \phi = \lambda$.

the values of the involved parameters, we have used suitable finite values of $\eta \to \infty$, as $\eta = \eta_\infty = 3$ *to* 6. For the computation of the numerical solution, we have selected the following fixed values of involved parameters $M = 0.1$, $\Pr = 6.2$, $K = 0.5$, $\phi = 0.1$, $m_0 = 0.5$, $B_i = 0.5$, $S_c = 3$.

Tables 2 and 3 are erected numerically to validate our presented results by fixing values of different parameters. It is found that all obtained results are in good alignment to those given in Reddy[41] and Cortell[42].

The impact of solid volume fraction ϕ on axial velocity, microrotation and temperature distributions is depicted in Figs 2–4. Figure 2 shows that the axial velocity profile decline versus increasing values of volume fraction. The effect of ϕ on microrotation profile is given in Fig. 3. It is perceived that the microrotation profile decays near and grows far away from the boundary layer and satisfies it asymptotically. While the temperature distribution diminishes, and its associated thermal boundary layer thickness augments when values of ϕ are increased as given in Fig. 4.

Figures 5–7 examine the effect of micropolar material parameter K on axial velocity, microrotation, and temperature profiles. Figure 5 demonstrates the effect of K on velocity field. It is witnessed that the velocity field and momentum boundary layer augment versus growing values of the K. This is because of the reason that viscosity declines with growing the values of K. Due to this low viscosity, the temperature distribution also decreases which is illustrated in Fig. 6. Moreover, the value of microrotation velocity at the wall diminishes continuously from maximum to zero far away from the wall as illustrated in Fig. 7.

Figures 8–10 outline the behavior of axial velocity, microrotation velocity, and temperature profile for different values of the magnetic parameter M respectively. Figures 8 and 9 display the impact of M on axial velocity and temperature distribution. It is witnessed that for higher the values of M, the velocity profile declines whereas temperature field and thermal boundary layer thickness increase. Actually, the increase in values of M means stronger Lorentz force which offers more resistance to the fluid's motion. That is why decline in fluid's velocity is witnessed. Also, because of this fact more heat is produced and as a result, the temperature profile and thermal boundary layer thickness are increased. Figure 10 shows the impact of magnetic parameter M on microrotation velocity. For gradually mounting values of magnetic parameter M, the microrotation velocity profile diminishes near the boundary and an opposite behavior is observed far-off from the boundary.

Figures 11–14 analyze the axial velocity, microrotation velocity, temperature and concentration fields for numerous values of power-law index parameter n respectively. Figure 11 depicts the upshot of n on velocity field. It is witnessed that the velocity distribution rises when values of n are increased. This is due to the fact that enhanced values of n are the main cause for the decrease in the thickness of the wall and as a result, more stretching of the sheet is observed which is responsible for enhanced velocity. However, the microrotation velocity and temperature profiles diminish by enhancing the values of n as given in Figs 12 and 13 respectively. Figure 14 illustrates the concentration profile for numerous values of n. It is seen that for the higher values of power-law index parameter n, the concentration field boosts.

Figure 15 specifies the microrotation velocity field for distinct values of boundary parameter m_0. It is noticed that the microrotation velocity profile is enhanced for growing values of m_0. Figure 16 is graphed to perceive

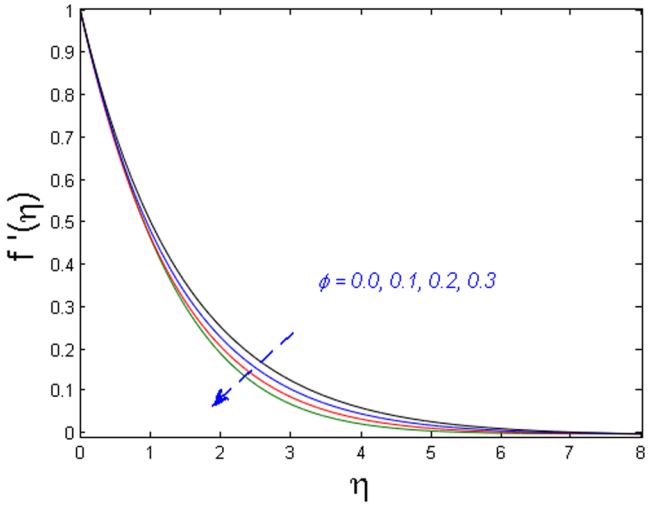

Figure 2. Effect of ϕ on $f'(\eta)$.

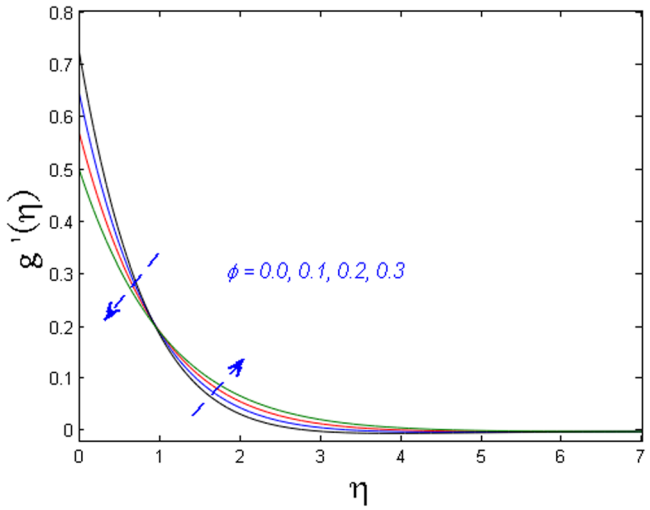

Figure 3. Effect of ϕ on $g'(\eta)$.

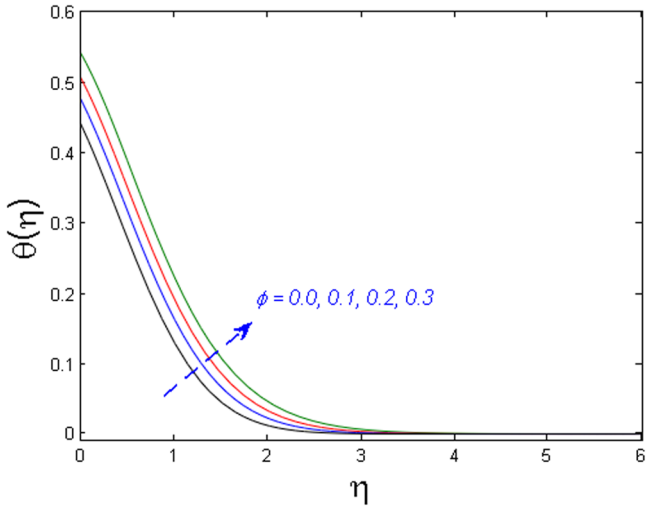

Figure 4. Effect of ϕ on $\theta(\eta)$.

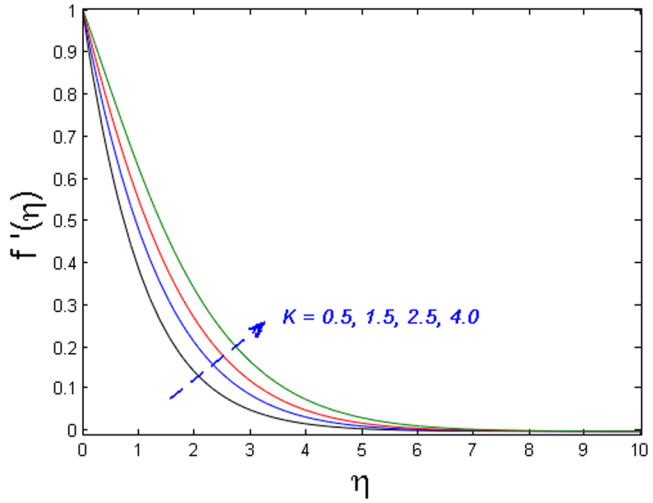

Figure 5. Effect of K on $f'(\eta)$.

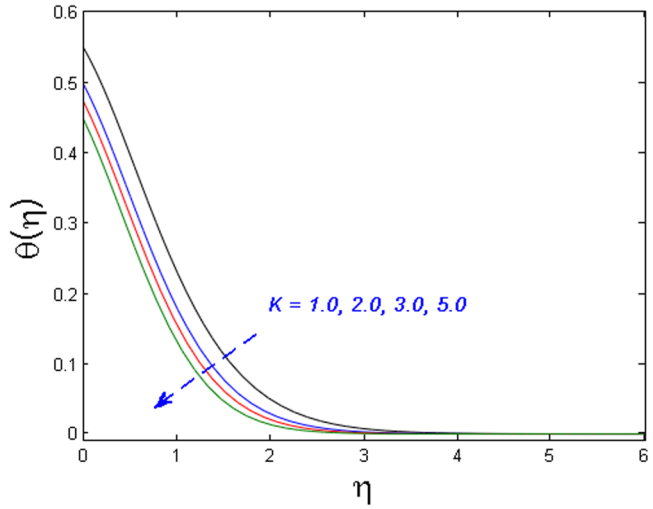

Figure 6. Effect of K on $\theta(\eta)$.

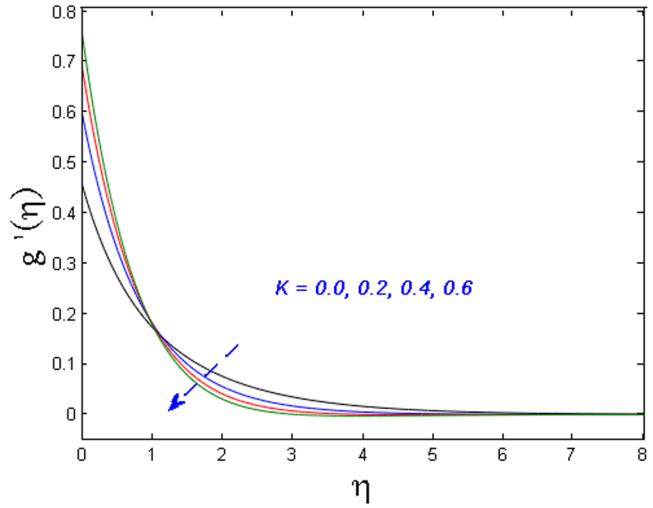

Figure 7. Effect of K on $g'(\eta)$.

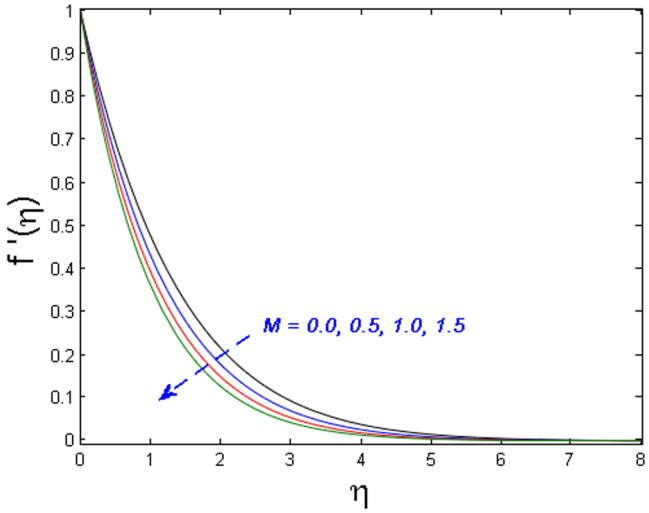

Figure 8. Effect of M on $f'(\eta)$.

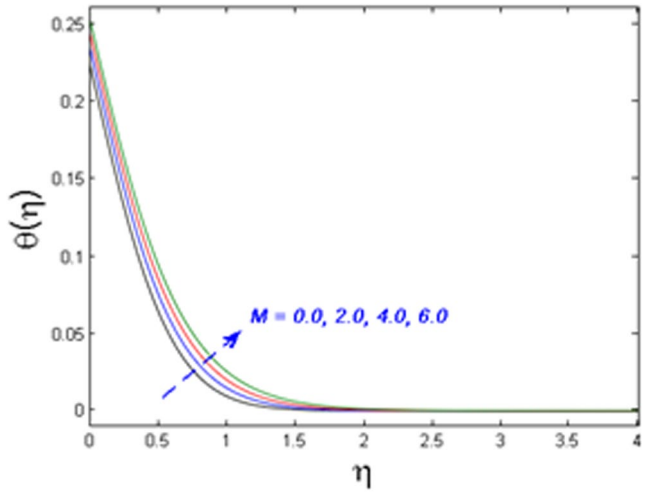

Figure 9. Effect of M on $\theta(\eta)$.

the variation in temperature profile for different values of Biot number B_i. It is seen that temperature profile is increased for growing estimations of Biot number. It is due to the fact that increasing values of Biot number B_i rises the heat transfer coefficient which ultimately enhances the temperature. The action of γ (heat generation parameter) on the temperature profile is portrayed in Fig. 17. For increasing values of heat generation parameter γ means $T_w > T_\infty$ *i.e.*, more heat transfer from the surface to the fluid and as a result, the fluid temperature is enhanced. Figures 18 and 19 portrayed to depict the influence of radiation parameter R_d and temperature ratio parameter θ_w on temperature field respectively. It is apparent from the figure that the temperature field is higher for values of both the radiation parameter and temperature ratio parameter. Physically this is due to the fact that with the increase in radiation parameter, the mean absorption coefficient decreases. Hence the rate of radiative heat transfers to the fluid increases.

Figure 20 specifies the concentration profile for varying values of Schmidt number S_c. As we know that the Schmidt number is inversely proportional to mass diffusivity. That is why concentration distribution enhances and its corresponding boundary layer thickness diminishes versus gradual increasing values of the S_c. In Fig. 21 impact of the strength of homogeneous reaction k_1 on concentration field is described. As the reactants are depleted in a chemical reaction. Because of this fact concentration field shows decreasing the tendency for improving values of k_1. From Fig. 22, it is noticed that concentration distribution is the decreasing function of the strength of heterogeneous reaction k_2. Higher values of k_2 weaken the diffusion coefficient and as a result, less diffused particles abate the concentration field.

Finally, the effect of physical quantities of interest such as the Skin friction coefficient and the Nusselt number for various values of dimensionless governing flow field parameters are graphed in Figs 23–26 respectively. Figure 23 portrays the impact on Skin friction coefficient $\mathrm{Re}_x^{1/2} C_f$ for various values of Biot number B_i and solid volume fraction ϕ. It can be seen that the Skin friction coefficient decreases versus augmented values of the Biot

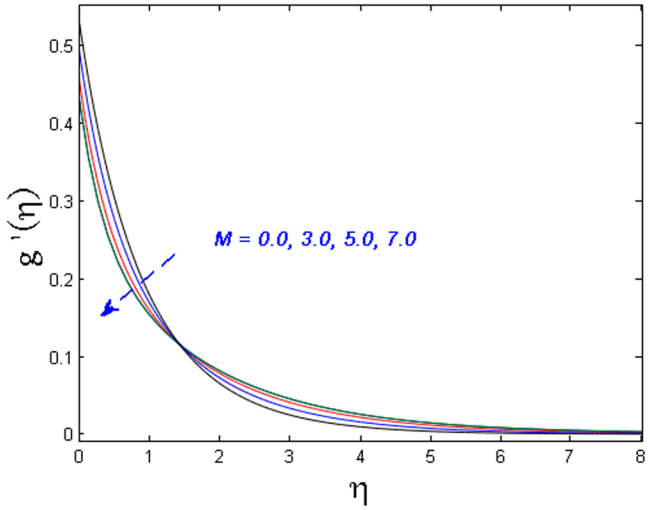

Figure 10. Effect of M on $g'(\eta)$.

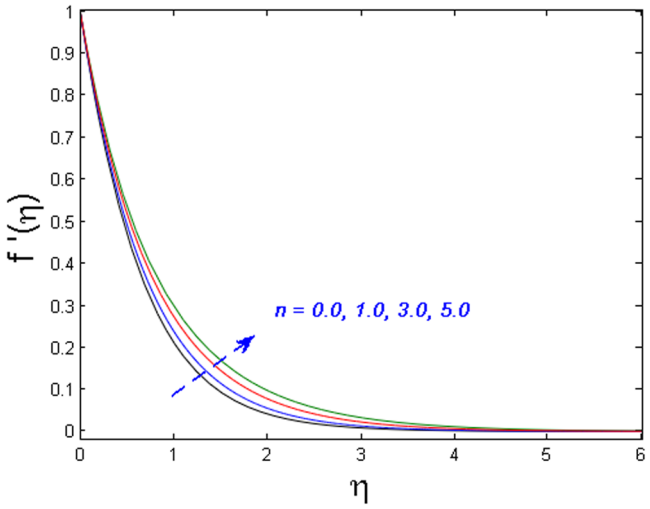

Figure 11. Effect of n on $f'(\eta)$.

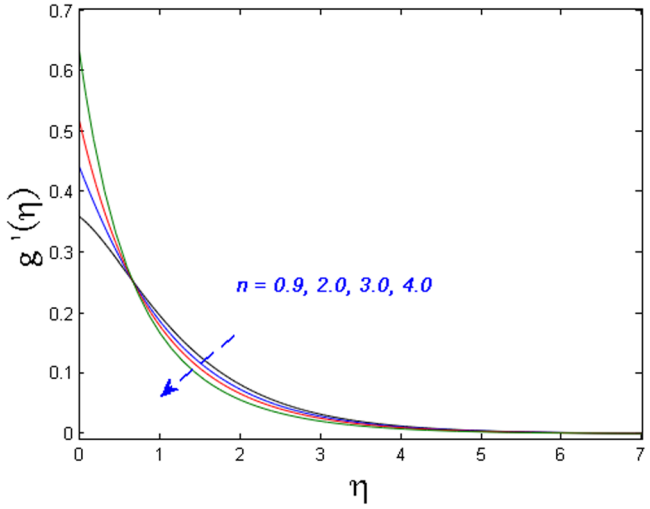

Figure 12. Effect of n on $g'(\eta)$.

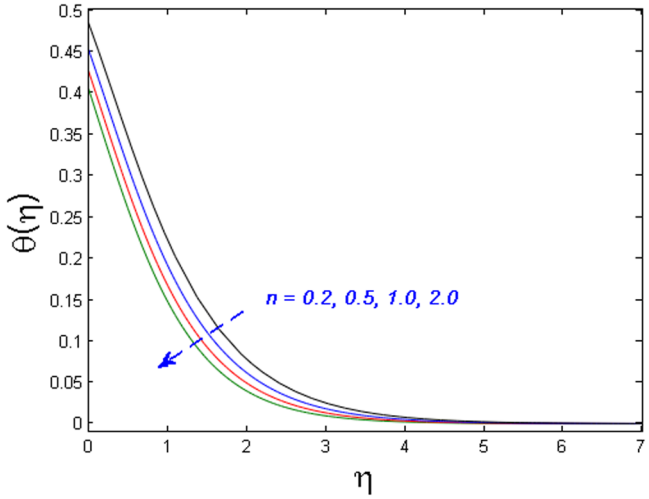

Figure 13. Effect of n on $\theta(\eta)$.

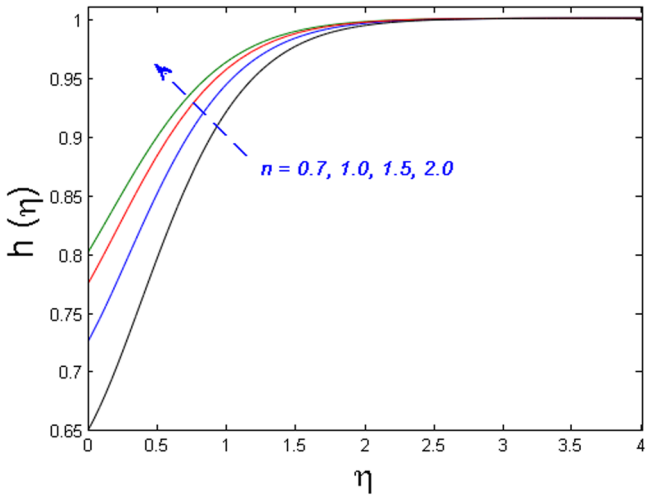

Figure 14. Effect of n on $h(\eta)$.

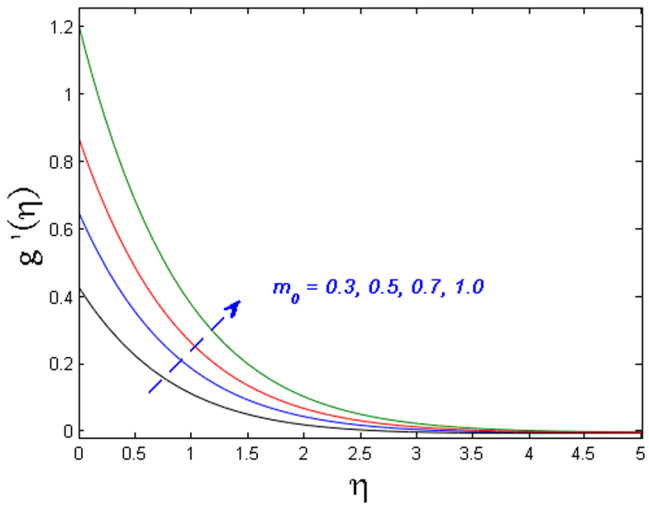

Figure 15. Effect of m_0 on $g'(\eta)$.

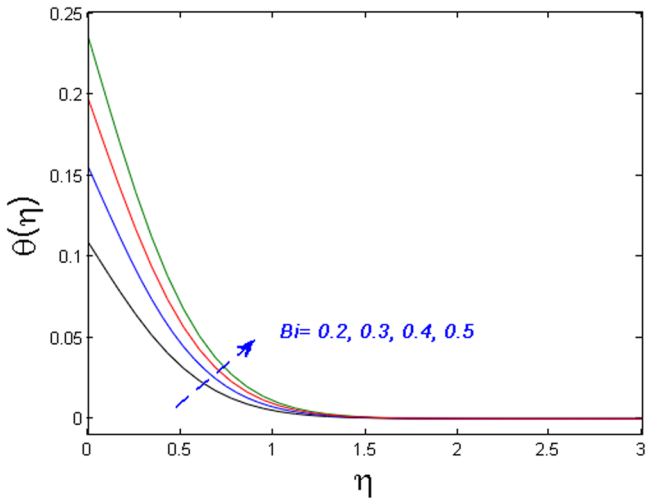

Figure 16. Effect of B_i on $\theta(\eta)$.

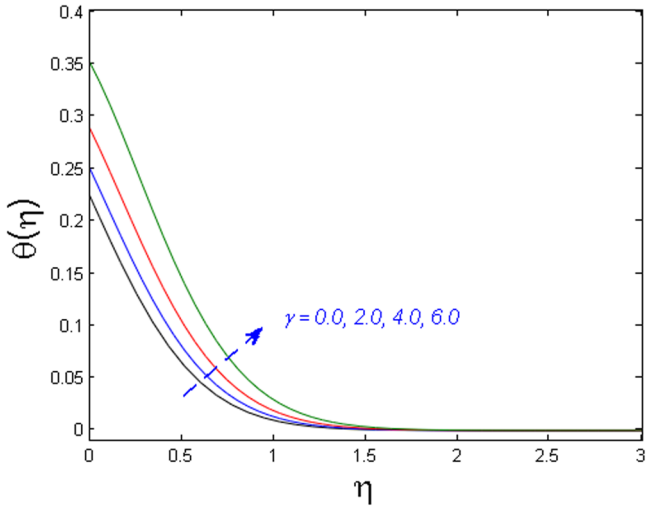

Figure 17. Effect of γ on $\theta(\eta)$.

number B_i and an opposite behavior are observed in case of solid volume fraction ϕ. Figure 24 displays effect on the Skin friction coefficient for varied estimated values of the magnetic parameter M and solid volume fraction ϕ. It is observed that the skin friction coefficient enhances for escalating values of the magnetic parameter and solid volume fraction ϕ. Figure 25 demonstrates the effect of the magnetic parameter and the volume fraction on the Nusselt number. It is found that the Nusselt number diminishes with enhancing the value of magnetic parameter however the contradictory impact is observed in the case of volume fraction parameter. Further, the Nusselt number increases with increasing the Biot number and the volume fraction parameter. This effect is displayed in Fig. 26.

Table 4 is erected to display the numerical values of Nusselt number $\mathrm{Re_x}^{-1/2}Nu_x$ for the varied values of the different parameter. It is seen that Nusselt number increases and Skin friction coefficient decrease for growing values of solid volume fraction ϕ and radiation parameter R_d. By mounting the values of heat generation parameter (γ), the Nusselt number diminishes while it enhances for increasing values of Biot number B_i. Moreover, the skin friction coefficient diminishes with enhancing the value of Biot number and it has no effect on skin coefficient with increasing the value of heat generation parameter. Table 5 depicts the behavior of $h'(0)$ and $\varphi'(0)$ when $\delta = 1$. It is witnessed that for increasing values of k_2, both $h'(0)$ and $\varphi'(0)$ show increasing behavior.

Concluding Remarks

In this article, a numerical solution for the effects of h-h reactions on the flow of micropolar nanofluid with water as the base fluid and Ferric oxide as nanoparticles past a nonlinear stretched surface is obtained and discussed. Additional impacts like nonlinear thermal radiation, magnetohydrodynamics, and heat generation/absorption with convective boundary condition are added features towards the novelty of the problem. The transformed

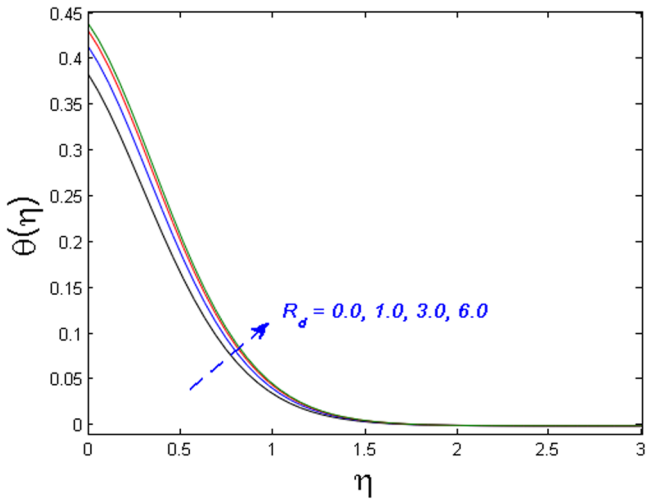

Figure 18. Effect of R_d on $\theta(\eta)$.

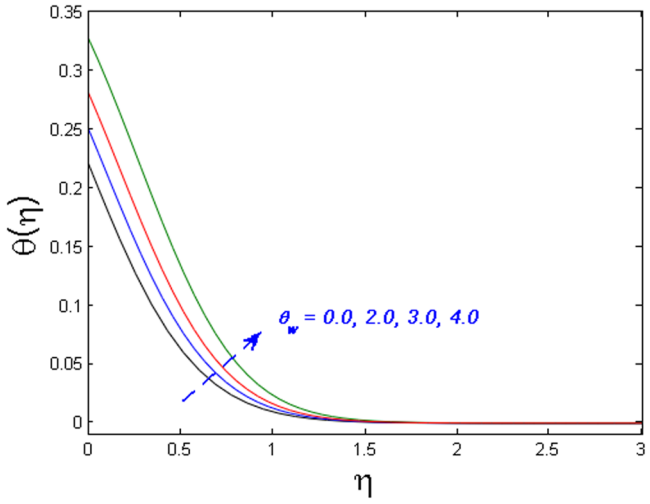

Figure 19. Effect θ_w on $\theta(\eta)$.

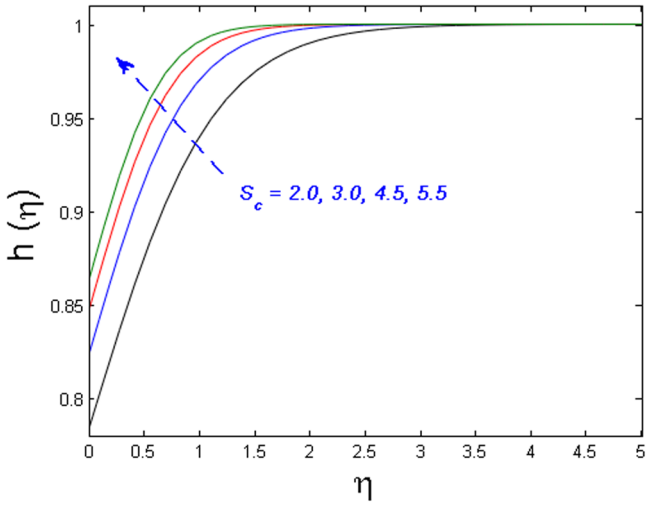

Figure 20. Effect of S_c on $h(\eta)$.

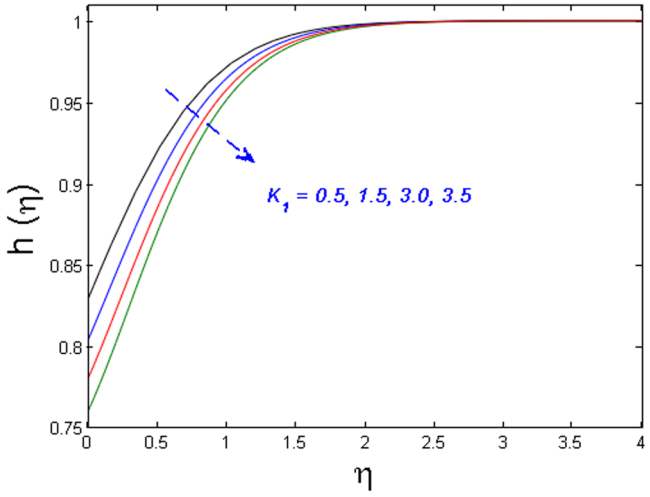

Figure 21. Effect of K_1 on $h(\eta)$.

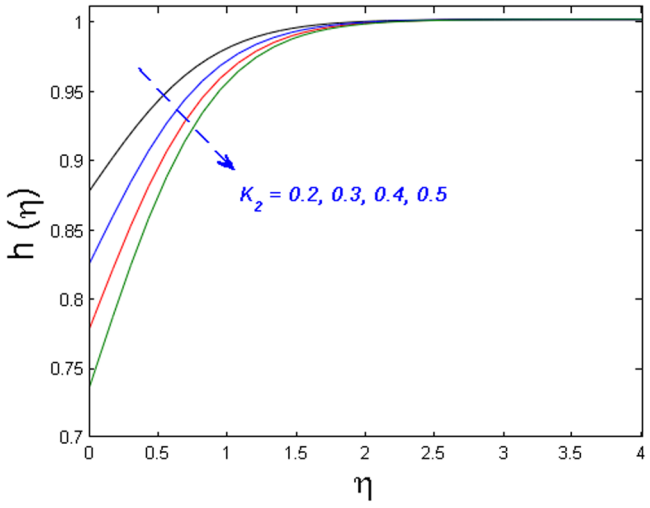

Figure 22. Effect of of K_2 on $h(\eta)$.

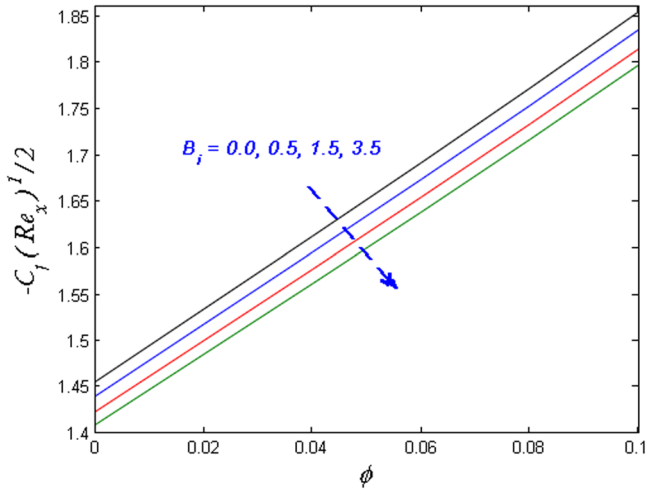

Figure 23. Effects of ϕ and B_i on $\mathrm{Re}_x^{1/2} C_f$.

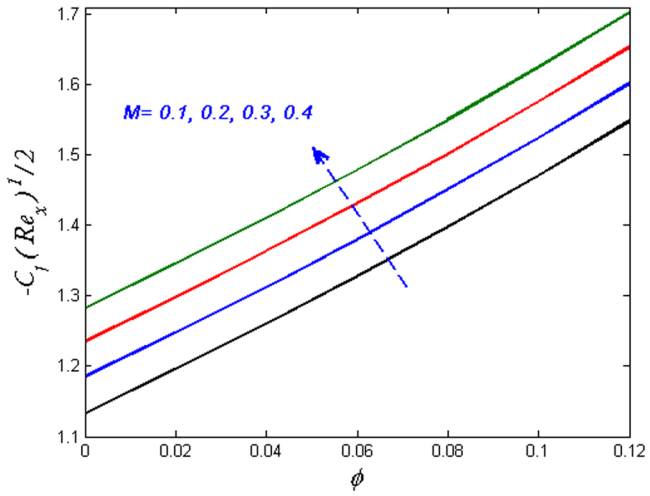

Figure 24. Effects of ϕ and M on $\mathrm{Re}_x^{1/2} C_f$.

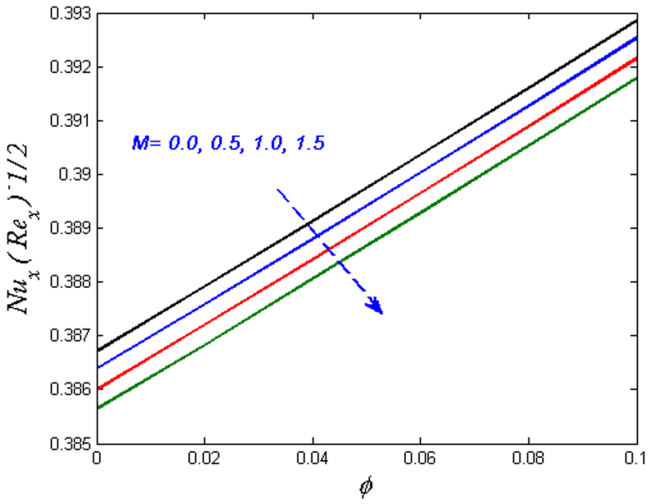

Figure 25. Effects of ϕ and M on $\mathrm{Re}_x^{-1/2} Nu_x$.

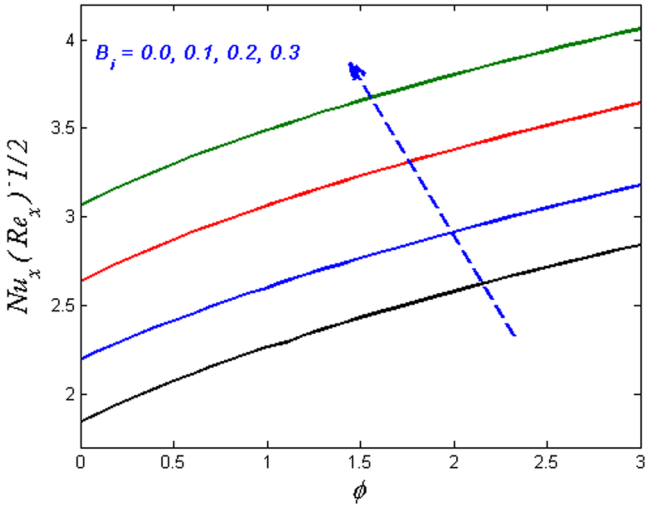

Figure 26. Effects of ϕ and B_i on $\mathrm{Re}_x^{-1/2} Nu_x$.

ϕ	R_d	γ	B_i	$\mathrm{Re}_x^{-1/2}Nu_x$	$\mathrm{Re}_x^{1/2}C_f$	$g'(0)$
0.1	03	0.1	0.5	1.70870	1.14570	0.62173
0.2				1.73360	1.11390	0.51651
0.3				1.76080	1.06140	0.42920
0.1	0.3	0.1	0.5	0.53758	1.14640	0.62174
	01			0.84084	1.14600	0.62174
	02			1.27460	1.14580	0.62173
0.1	03	0.1	0.5	1.70870	1.14570	0.62173
		0.3		1.61730	1.14570	0.62164
		0.5		1.38010	1.14570	0.62133
0.1	03	0.1	0.5	1.70870	1.14570	0.62173
			1.0	2.89670	1.13450	0.62164
			1.5	3.74190	1.12700	0.62157

Table 4. Numerical values of Nusselt number $\mathrm{Re}_x^{-1/2}Nu_x$, skin friction $\mathrm{Re}_x^{1/2}C_f$ and $g'(0)$ when $\theta_w = 1.2$, and $\mathrm{Pr} = 6.2$.

k_2	$h'(0)$	$-\varphi'(0)$
0.2	0.16977	0.16977
0.3	0.23660	0.23660
0.4	0.29451	0.29451
0.5	0.34515	034515

Table 5. Numerical values of $h'(0)$ and $-\varphi'(0)$ for different values of k_2 when $\delta = 1$.

system of ordinary differential equations is solved by MATLAB built-in function bvp4 for varied values of arising parameters. The salient points of the present study are given as follows:

- The velocity distribution with its associated boundary layer thickness increase for enhanced values of micropolar parameter K while the temperature profile and microrotation velocity diminish.
- For higher values of k_1 and k_2 (strength of homogeneous and heterogeneous reactions), concentration profile reduces.
- For gradually mounting values of magnetic parameter M, the microrotation velocity profile contracts near the boundary and opposite trend are witnessed far away from the boundary.
- The Nusselt number and Skin friction coefficient increase and decrease for growing values of solid volume fraction ϕ and radiation parameter R_d respectively.

References

1. Hayat, T., Muhammad, T., Shehzad, S. A. & Alsaedi, A. Similarity solution to three dimensional boundary layer flow of second grade nanofluid past a stretching surface with thermal radiation and heat source/sink. *AIP Adv.* **5**(1), 017107 (2015).
2. Sakiadis, B. C. Boundary layer behaviour on continuous solid surface I, The boundary layer equation for two dimensional and asymmetric flow. *AIChE J.* **7**, 26–28 (1961).
3. Crane, L. J. Flow past a stretching plate. *J. Appl Math Phys.* **21**, 645–647 (1970).
4. Gupta, P. S. & Gupta, A. S. Heat and Mass Transfer on a stretching sheet with suction and blowing. *Can. J Chem Eng.* **55**, 744–746 (1977).
5. Chakrabarti, A. & Gupta, A. S. Hydromagnetic flow and heat transfer over a stretching sheet. *Q. Appl. Math.* **37**, 73–78 (1979).
6. Devi, S. A. & Ganga, B. Dissipation effects on MHD nonlinear flow and heat transfer past a porous surface with prescribed heat flux. *J. Appl Fluid Mech.* **3**(1), 1–6 (2010).
7. Hsiao, K. L. Heat and mass mixed convection for MHD viscoelastic fuid past a stretching sheet with ohmic dissipation. *Commun. Nonlinear Sci Num Simul.* **15**(7), 1803–1812 (2010).
8. Ibrahim, W., Shankar, B. & Nandeppanavar, M. M. MHD stagnation point flow and heat transfer due to nanofluid towards a stretching sheet. *Int. J Heat Mass Tran.* **56**, 1–9 (2013).
9. Lin, Y., Zheng, L. & Chen, G. Unsteady flow and heat transfer of pseudo-plastic nano-liquid in a finite thin film on a stretching surface with variable thermal conductivity and viscous dissipation. *Powder. Technol.* **274**, 324–332 (2015).
10. Hsiao, K. L. Stagnation electrical MHD nanofluid mixed convection with slip boundary on a stretching sheet. *Appl. Therm Eng.* **98**, 850–861 (2016).
11. Hayat, T., Mustafa, M. & Asghar, S. Unsteady flow with heat and mass transfer of a third grade fluid over a stretching surface in the presence of chemical reaction. *Nonlinear Anal: Real World Appl.* **11**(4), 3186–3197 (2010).
12. Malvandi, A., Hedayati, F. & Ganji, D. D. Slip effects on unsteady stagnation point flow of a nanofluid over a stretching sheet. *Powder. Technol.* **253**, 377–384 (2014).
13. Khalili, S., Dinarvand, S., Hosseini, R., Tamim, H. & Pop, I. Unsteady MHD flow and heat transfer near stagnation point over a stretching/shrinking sheet in porous medium filled with a nanofluid. *Chinese. Phys B.* **23**, 048203 (2014).
14. Hayat, T., Iqbal, Z., Mustafa, M. & Alsaedi, A. Unsteady flow and heat transfer of Jeffrey fluid over a stretching sheet. *Therm. Sci.* **18**(4), 1069–1078 (2014).
15. Hayat, T., Asad, S., Mustafa, M. & Alsaedi, A. Radiation effects on the flow of Powell-Eyring fluid past an unsteady inclined stretching sheet with non-uniform heat source/sink. *PloS. One.* **9**(7), e103214 (2014).

16. Ahmadi, A. R., Zahmatkesh, A., Hatami, M. & Ganji, D. D. A comprehensive analysis of the flow and heat transfer for a nanofluid over an unsteady stretching flat plate. *Powder. Technol.* **258**, 125–133 (2014).
17. Chen, S., Zheng, L., Shen, B. & Chen, X. Time—space dependent fractional boundary layer flow of Maxwell fluid over an unsteady stretching surface. *Theor. Appl Mech Lett.* **5**(6), 262–266 (2015).
18. Hua, H. & Su, X. Unsteady MHD boundary layer flow and heat transfer over the stretching sheets submerged in a moving fluid with Ohmic heating and frictional heating. *Open. Phys.* **13**(1), 210–217 (2015).
19. Hayat, T., Shafiq, A., Alsaedi, A. & Shahzad, S. A. Unsteady MHD flow over exponentially stretching sheet with slip conditions. *Appl. Math Mech.* **37**(2), 193–208 (2016).
20. Waqas, M. *et al*. Magnetohydrodynamic (MHD) mixed convection flow of micropolar liquid due to nonlinear stretched sheet with convective condition. *Int. J Heat Mass Tran.* **102**, 766–772 (2016).
21. Lu, D., Ramzan, M., ul Huda, N., Chung, J. D. & Farooq, U. Nonlinear radiation effect on MHD Carreau nanofluid flow over a radially stretching surface with zero mass flux at the surface. *Sci. Rep.* **8**(1), 3709 (2018).
22. Khan, M. I., Hayat, T., Khan, M. I. & Alsaedi, A. A modified homogeneous-heterogeneous reaction for MHD stagnation flow with viscous dissipation and Joule heating. *Int. J Heat Mass Tran.* **113**, 310–317 (2017).
23. Hayat, T., Sajjad, R., Ellahi, R., Alsaedi, A. & Muhammad, T. Homogeneous-heterogeneous reactions in MHD flow of micropolar fluid by a curved stretching surface. *J. Mol Liq.* **240**, 209–220 (2017).
24. Lu, D. *et al*. On three-dimensional MHD Oldroyd-B fluid flow with nonlinear thermal radiation and homogeneous–heterogeneous reaction. *J. Brazilian Soc. Mech. Sci. Eng.* **40**(8), 387 (2018).
25. Abbas, Z. & Sheikh, M. Numerical study of homogeneous–heterogeneous reactions on stagnation point flow of ferrofluid with non-linear slip condition. *Chinese. J Chem Eng.* **25**(1), 11–17 (2017).
26. Nadeem, S., Ullah, N., Khan, A. U. & Akbar, T. Effect of homogeneous-heterogeneous reactions on ferrofluid in the presence of magnetic dipole along a stretching cylinder. *Results. Phys.* **7**, 3574–3582 (2017).
27. Prakash, J., Raju, C. S. K. & Sandeep, N. Dual solutions for heat and mass transfer in MHD Jeffrey fluid in the presence of homogeneous-heterogeneous reactions. *Front. Heat Mass Transfer.* **7**(1), 14 (2016).
28. Khan, I., Malik, M. Y., Hussain, A. & Salahuddin, T. Effect of homogenous-heterogeneous reactions on MHD Prandtl fluid flow over a stretching sheet. *Results. Phys.* **7**, 4226–4231 (2017).
29. Choi, S. U., & Eastman, J. A. *Enhancing thermal conductivity of fluids with nanoparticles*. No. ANL/MSD/CP–84938; CONF-951135–29. Argonne National Lab., IL (United States, 1995).
30. Keblinski, P., Eastman, J. A. & Cahill, D. G. Nanofluids for thermal transport. *Mater. Today.* **8**, 36–44 (2005).
31. Wong, K. V., & De Leon, O. Applications of nanofluids: current and future. *Adv. Mech Eng*. (2010).
32. Nadeem, S. & Muhammad, N. Impact of stratification and Cattaneo-Christov heat flux in the flow saturated with porous medium. *J. Mol Liq.* **224**, 423–430 (2016).
33. Nadeem, S. & Lee, C. Boundary layer flow of nanofluid over an exponentially stretching surface. *Nanoscale. Res Lett.* **79**(1), 94 (2012).
34. Sheikholeslami, M. Numerical investigation of nanofluid free convection under the influence of electric field in a porous enclosure. *J. Mol Liq.* **249**, 1212–1221 (2018).
35. Nadeem, S., Riaz, A., Ellahi, R. & Akbar, N. S. Effects of heat and mass transfer on peristaltic flow of a nanofluid between eccentric cylinders. *Appl. Nanosci.* **4**(4), 393–404 (2014).
36. Sheikholeslami, M., Soleimani, S. & Ganji, D. D. Effect of electric field on hydrothermal behavior of nanofluid in a complex geometry. *J. Mol Liq.* **213**, 153–161 (2016).
37. Raju, C. S., Jayachandra Babu, M. & Sandeep, N. Chemically reacting radiative MHD Jeffrey nanofluid flow over a cone in porous medium. *Int. J Eng Res Africa.* **19**, 75–90 (2016).
38. Merkin, J. H. A model for isothermal homogeneous-heterogeneous reactions in boundary-layer flow. *Math. Compu Model.* **24**(8), 125–136 (1996).
39. Chaudhary, M. A. & Merkin, J. H. A simple isothermal model for homogeneous-heterogeneous reactions in boundary-layer flow. I Equal diffusivities. *Fluid. Dyn Res.* **16**(6), 311–333 (1995).
40. Chaudhary, M. A. & Merkin, J. H. A simple isothermal model for homogeneous-heterogeneous reactions in boundary-layer flow. *II Equal diffusivities. Fluid. Dyn Res.* **16**(6), 335 (1995).
41. Reddy, M. G. Influence of Lorentz force, Cattaneo-Christov heat flux and viscous dissipation on the flow of micropolar fluid past a nonlinear convective stretching vertical surface. *Nonlin. Eng.* **6**(4), 317–326 (2017).
42. Cortell, R. Viscous flow and heat transfer over a nonlinearly stretching sheet. *Appl. Math Comp.* **184**(2), 864–873 (2007).

Acknowledgements

This work was supported by the Korea Institute of Energy Technology Evaluation and Planning (KETEP) and the Ministry of Trade, Industry & Energy(MOTIE) of the Republic of Korea (No. 20172010105570).

Author Contributions

D.L. and M.R. worked on the Mathematical model and its numerical solution. However, S.A., J.D.C. and U.F. wrote the manuscript and prepared the figures.

Additional Information

Competing Interests: The authors declare no competing interests.

Publisher's note: Springer Nature remains neutral with regard to jurisdictional claims in published maps and institutional affiliations.